Gilles Bourque
Rolls-Royce Canada,
Montreal, H9P 1A5, Canada

Darren Healy

Henry Curran

Department of Chemistry,
National University of Ireland,
Galway, Ireland

Christopher Zinner

Danielle Kalitan

Department of Mechanical, Materials, and
Aerospace Engineering,
University of Central Florida,
Orlando, FL 32816

Jaap de Vries

Christopher Aul

Eric Petersen
Department of Mechanical Engineering,
Texas A&M University,
College Station, TX 77843

Ignition and Flame Speed Kinetics of Two Natural Gas Blends With High Levels of Heavier Hydrocarbons

High-pressure experiments and chemical kinetics modeling were performed to generate a database and a chemical kinetic model that can characterize the combustion chemistry of methane-based fuel blends containing significant levels of heavy hydrocarbons (up to 37.5% by volume). Ignition delay times were measured in two different shock tubes and in a rapid compression machine at pressures up to 34 atm and temperatures from 740 K to 1660 K. Laminar flame speeds were also measured at pressures up to 4 atm using a high-pressure vessel with optical access. Two different fuel blends containing ethane, propane, n-butane, and n-pentane added to methane were studied at equivalence ratios varying from lean (0.3) to rich (2.0). This paper represents the most comprehensive set of experimental ignition and laminar flame speed data available in the open literature for $CH_4/C_2H_6/C_3H_8/C_4H_{10}/C_5H_{12}$ fuel blends with significant levels of C2+ hydrocarbons. Using these data, a detailed chemical kinetics model based on current and recent work by the authors was compiled and refined. The predictions of the model are very good over the entire range of ignition delay times, considering the fact that the data set is so thorough. Nonetheless, some improvements to the model can still be made with respect to ignition times at the lowest temperatures and for the laminar flame speeds at pressures above 1 atm and at rich conditions. [DOI: 10.1115/1.3124665]

1 Introduction

Fuel-flexible gas turbine engines are presently of interest to the power generation and combustion research communities because variations in fuel composition are expected to increase. Such variations can be due to dissimilarities in the fuel source itself or to the advent of alternative fuels currently being developed at a fast pace. Varying fuel compositions of primary interest herein are the result of heavier hydrocarbons present in a methane-based fuel [1]. The additional hydrocarbons reside in the fuel blend as an additive or extender to a conventional fuel; as a fuel component already present in the fuel blend for various reasons; or as a fuel in its own right. One important physical parameter characterizing the chemistry of a fuel blend is its ignition delay time. This delay time is both a fundamental parameter for the development of detailed kinetics mechanisms and a practical constraint for premixed combustion. For example, residence times for premixed fuel-air compositions need to be below the mixture's autoignition time at a given temperature and pressure [2].

Additionally, the unsteady flame stretch and strain, related to the Markstein length and the Strouhal number, are known to play important roles in flame dynamics [3]. Since the Markstein length is markedly different for the different hydrocarbon species present in natural gas, the chemical kinetics modeling of the effect of natural gas composition on flame characteristics is important to understanding the flame dynamics leading to thermoacoustic instability in gas turbine combustion systems. Flame stretch is related to laminar flame speed, a fundamental parameter of a given mixture composition, stoichiometry, temperature, and pressure [4].

In a recent paper, the authors used a chemical kinetics mechanism to explore the ignition delay time and flame speed variations for a few specific natural gas blends at practical engine conditions [1]. Several studies have been performed in the past for methane-based fuel blend ignition [5–12], but most of these were at relatively low pressures and dealt with relatively small levels of hydrocarbon additives. More recently, the authors have been studying the effect of hydrocarbons on methane ignition in both shock tubes and rapid compression machines (RCMs) [13–18]. While the laminar flame speed of pure methane can be considered well known [19–22], there are few studies with laminar flame speed measurements of methane blends, particularly at elevated pressures and for 20% or more heavy hydrocarbons present in the fuel mixture [1]. Further details on related studies from the literature are presented in Refs. [1,13].

This paper addresses the topic of fuel-flexible natural gas combustion and extends the work presented in Ref. [1] to include an extensive combination of experimental data and kinetics modeling for natural gas blends with relatively large levels of heavy hydrocarbons. Table 1 presents the three target mixtures of interest, with mixtures NG2 and NG3—the two with less than 82% methane—being the focus of the present study. Ignition experiments from two different types of facilities, shock tube, and rapid compression machine, were performed at pressures between 1 atm and 30 atm for a range of temperatures between approximately 700 K and 1600 K. Details on the experiments and the corresponding results are presented and compared with a new chemical kinetics model

Contributed by the International Gas Turbine Institute of ASME for publication in the JOURNAL OF ENGINEERING FOR GAS TURBINES AND POWER. Manuscript received April 4, 2008; final manuscript received May 22, 2008; published online October 30, 2009. Review conducted by Dilip R. Ballal. Paper presented at the ASME Turbo Expo 2008: Land, Sea and Air (GT2008), Berlin, Germany, June 9–13, 2008.

Table 1 Mixture compositions in percent volume

Species	NG1 (%)	NG2 (%)	NG3 (%)
CH_4	98.125	81.25	62.5
C_2H_6	1.000	10.00	20.0
C_3H_8	0.500	5.00	10.0
nC_4H_{10}	0.250	2.50	5.0
nC_5H_{12}	0.125	1.25	2.5

designed specifically for methane-based fuel blends containing hydrocarbons with as many as five carbon atoms. High-pressure laminar flame speed experiments were also performed for NG2 and NG3, the results of which are presented below and compared with the predictions of the chemical kinetics model. No study was found in the literature that has covered such a thorough range of conditions, data type, mixture composition, and detailed kinetics modeling for natural gas blends, as presented in this paper.

2 Chemical Kinetics Model

The detailed chemical kinetic model is based on the hierarchical nature of hydrocarbon combustion mechanisms containing the H_2/O_2 submechanism, together with the CO/CH_4 and larger hydrocarbon submechanisms and is similar to, but not identical to that published in our previous work on methane/propane mixtures [14]. Some changes have been made and these are discussed here. We have adopted the rate constant of Hessler [23] for $H+O_2 \rightarrow O+OH$, but this has had little effect on the predictions. You et al. [24] recently reported on the rate constant for $CO+HO_2$, and we have adopted their value.

Recently, Srinivasan et al. [25] studied the reaction $CH_4+O_2 \rightarrow CH_3+HO_2$, and using both experimental results and calculations provided a rate constant in the temperature range 1655–1822 K. Jasper et al. [26] calculated a rate constant expression for $CH_3+HO_2 \rightarrow CH_3O+OH$, which we have also adopted. The rate constant expression for $C_2H_6+H \rightarrow C_2H_5+H_2$ was taken from GRI-MECH 3.0 [27].

Moreover, sensitivity analysis has shown that for the prediction of ignition delay times for methane, ethane, in particular, and propane fuels are very sensitive to the rate constant for the decomposition of ethyl radicals to ethylene and H atoms. We have adopted the rate constant expression recommended in GRI-MECH 3.0 [27], which is approximately a factor of 2 slower than the rate constant in our previous paper [14].

Rate constants for the C4 and C5 submechanisms are based on the reaction rate rules presented in the work on the primary reference fuels published by Curran et al. [28,29]. In particular, the reaction rate rules specified in the iso-octane paper are those used here. The mechanism comprises 289 species and 1580 reactions.

Other minor changes have been made to the mechanism, but the preceding description details the most significant changes. A full listing of the mechanism together with thermochemical parameters and transport data are available on the NUI Galway combustion chemistry website.[1]

The Premix program from CHEMKIN [30] was used to simulate the adiabatic freely propagating laminar flame. At temperatures greater than about 1000–1250 K, depending on the pressure, addition of alkyl radicals to molecular oxygen is no longer important, with β-scission and isomerization of fuel alkyl radicals dominating the oxidation process. Thus, in simulating flame speed measurements we generated a "high-temperature" mechanism from the full detailed mechanism described above by removing the low-temperature chemistry, i.e., $iC_4H_9O_2$ radicals and their subsequent low-temperature reactions are not included in the flame speed simulations.

Also, no species diffusion is included in the simulation. Verification of this assumption on a subset of the results showed no noticeable effect on the final results. Gradient and curvature parameters were set to values on the order of 0.1 to ensure appropriate flame zone resolution and the insensitivity of the resulting laminar flame speed to these parameters.

3 Ignition Delay Times

Presented in this section are the methods and results for the measurement of ignition delay times. Brief overviews of the shock-tube and RCM apparatuses are given first, followed by a detailed summary of the resulting data. The measured ignition times are compared with the predictions of the kinetics model, and shock-tube data and RCM data are shown on the same plots when overlapping data sets are available.

3.1 Apparatus and Procedure. Two high-pressure shock-tube facilities were employed for the experiments detailed herein. Key features of the shock tube of the first facility are a driven section having a length of approximately 10.7 m (35 ft) and an inner diameter of 16.2 cm with a driver section 3.5 m in length and inner diameter of 7.62 cm. The shock tube of the second facility has a driven section with an inner diameter of 15.24 cm and a length of 4.72 m with a diver section 4.93 m long and inner diameter of 7.62 cm.

Both shock-tube facilities are configured for optimum test conditions behind reflected-shock waves, and both possess the capability for reflected-region pressures on the order of 100 atmospheres with untailored experimental test times approaching 3 ms. Conditions in the quiescent region behind the reflected shock are determined by one-dimensional shock relations and the incident-shock velocity. The velocity of the incident shock is obtained by use of timer counters (Fluke PM 6666) linked to a series of sequential pressure transducers (PCB 113) at locations in the shock tube near the endwall of the driven section.

The presence of chemical reactions in the reflected-shock region is detected by pressure transducers (PCB 134A and Kistler 603B1) and photomultiplier tubes (Hamamatsu 1P21) located at the endwall of the driven section and at a sidewall location 1 cm from the endwall. For optical diagnostics of CH^* chemiluminescence, CaF_2 windows are installed at both the sidewall and endwall locations, and the emission past each window is focused through a 430 ± 5 nm bandpass filter onto photomultiplier tubes mounted in custom-made hardware. Data acquisition is handled by GAGESCOPE data acquisition boards and software with sampling rates of at least 1 MHz per channel and 14 bit resolution. Further details on the experimental hardware, physical layout, auxiliary components, and diagnostics of the first shock-tube facility are presented in Ref. [31] and of the second shock-tube facility in Ref. [32].

The NUI Galway rapid compression machine has a twin-opposed piston configuration, which has been described previously by Affleck and Thomas [33], resulting in a fast compression time of approximately 16 ms. Creviced piston heads are used to improve the postcompression temperature distribution in the combustion chamber [34]. Full details of the machine are provided in a recent work performed on propane oxidation at high pressures and low temperatures [35].

Experiments were carried out at a compression ratio, defined as the ratio between the volume before compression and at the end of compression, of approximately 10:1. The "effective" compression ratio is lower using argon compared with nitrogen as diluent gas due to its higher thermal diffusivity. In order to vary the compressed gas temperature, T_C, the proportions of the diluent gases (N_2, Ar) were varied to alter the overall heat capacity of the fuel and "air" mixture. In addition, an electrothermal digitally controlled heating blanket surrounds the combustion chamber such

[1] http://c3.nuigalway.ie/naturalgas2.html.

Table 2 RCM ignition delay time data for NG2

T_C (K)	p_C (atm)	τ_{ign} (ms)	ϕ
848	29.56	144.00	0.5
841	28.57	148.00	
896	29.06	95.80	
892	28.66	91.70	
926	27.67	57.60	
925	28.24	53.60	
925	29.11	46.52	
984	29.16	13.29	
984	29.14	12.99	
1047	29.37	3.98	
1049	29.53	3.96	
985	19.19	31.66	
985	19.21	37.67	
984	19.14	33.35	
1039	19.23	7.90	
1041	19.35	8.23	
1096	19.00	2.79	
1096	19.04	3.29	
1021	9.21	48.10	
1026	9.37	46.32	
1080	9.21	9.73	
1073	9.03	9.23	
1126	9.29	3.96	
1130	9.40	4.11	
739	29.83	212.8	1.0
741	30.15	185.0	
780	29.54	145.5	
781	29.68	146.3	
816	27.37	145.0	
817	26.38	152.1	
852	27.89	146.0	
850	28.82	127.0	
857	29.61	106.0	
857	29.54	110.0	
912	29.04	34.8	
908	28.86	50.6	
938	28.45	21.9	
989	28.18	21.3	
908	19.30	129.4	
909	19.27	129.2	
938	18.04	60.9	
939	18.90	73.6	
940	18.99	65.6	
991	18.96	9.5	
989	19.10	9.4	
1046	18.95	3.6	
1047	19.00	3.8	
984	9.26	42.8	
979	9.34	21.4	
1036	9.53	11.2	
1040	9.41	11.21	

that the initial temperature may be varied up to a maximum operating temperature of 393 K. In this way, compressed gas temperatures in the range 680–1050 K were studied.

Pressure-time data were measured using a pressure transducer (Kistler 603B) and transferred via an amplifier to an oscilloscope where they were recorded. The ignition delay time, defined as the time from the end of compression to the maximum rate of pressure rise during ignition, was measured using two vertical cursors on the oscilloscope. In general, we found that the ignition delay times were reproducible to within 10% of one another at each T_C, Table 2. The compressed gas pressure was measured using two horizontal cursors.

The primary experimental data comprised of the pressure-time record, but it was more practical to assimilate and present the results in terms of the overall dependence of ignition delay on the compressed gas temperature, Table 2.

Heat losses are always a consideration in performing RCM experiments, becoming increasingly important when ignition delay times become longer. Thus, each experiment is simulated starting with the initial temperature, pressure and mixture composition, and the appropriate compression ratio chosen such that the simulated compressed gas pressure matches that measured experimentally. The constant-volume portion of the experiment is simulated as an adiabatic expansion, such that the simulated pressure profile again reproduces the experimental measurement. For a more detailed discussed of this modeling approach please see the propane work of Gallagher et al. [35].

3.2 Ignition Results. An extensive database of ignition delay times was obtained for the NG2 and NG3 fuel blends in air. For the shock-tube measurements, the undiluted fuel-air mixtures produced very clear pressure increases at the onset of ignition for every experiment. The pressure increases were indicative of strong ignition events and are similar in appearance to those presented in Refs. [13,14]. For such pressure traces, the definition of ignition delay time is unambiguous, providing uncertainties in the definition of ignition delay time of less than 10% and typically on the order of only a few percent for ignition times greater than about 50 μs. Although sidewall pressure and emission traces were also obtained, the endwall traces were used exclusively to define the ignition delay times presented in Table 3 because ignition occurs first at the endwall and also because ignition at a sidewall location appears accelerated because of the strong ignition wave that forms at the endwall and moves away from it. The CH^* chemiluminescence data corroborated the ignition times obtained from the pressure data, and no pre-ignition or early emission was seen for the range of conditions of the shock-tube experiments herein.

The analysis of the RCM data provided in Table 2 is as described above, and the definition of ignition delay time is similar to that described previously [35]. In short, the ignition time was defined at the inflection point between the test pressure achieved after compressing the mixture and the steep rise in pressure at the time of ignition.

Overall, the breadth of the conditions for the ignition delay time data set is quite extensive, covering a combined range between the RCM and shock-tube experiments from 739 K to 1667 K and from 0.7 atm to 33.9 atm. In general, the RCM data cover the lower-temperature range, while the shock-tube data cover the higher-temperature range. Fuel-to-air equivalence ratios (ϕ) of 0.3, 0.5, 1.0, and 2.0 were tested for both fuel mixtures. Each series of data within a similar grouping of pressure was compared with predictions from the chemical kinetics model described above. These calculations were performed using the Hydrodynamics, Chemistry and Transport (HCT) program [36] at conditions of constant volume and constant internal energy to model the pressure increase due to reaction.

Results for both shock-tube and RCM experiments are available for the NG2 blend for ϕ=0.5 and 1.0, shown in Figs. 1 and 2, respectively. For the lean results in Fig. 1, the RCM and shock-tube data align nicely for common pressures. Notable also is the good agreement between model and data over most of the temperature range. At the lowest temperatures for the 20 atm and 30 atm RCM data, the model underpredicts slightly the ignition delay times, but nevertheless the model reproduces the nonlinear trends seen in the data at the lowest temperatures and highest pressures. Similar trends are seen in Fig. 2 for the stoichiometric data among the two techniques and the model predictions.

Further comparisons between model and data for NG2 are shown in Figs. 3 and 4. For the leanest case, ϕ=0.3 in Fig. 3, the agreement between the model and shock-tube data is good, but some improvements can still be made at 8 atm and 30 atm. At the rich ϕ=2.0 condition in Fig. 4, the agreement between model and data is quite good, particularly at 15 atm.

Shock-tube ignition delay time data for NG3 are shown in Figs.

Table 3 Shock-tube ignition delay time data for NG2 and NG3

T (K)	p (atm)	τ_{ign} (μs)	ϕ
	Natural gas blend 2		
1099	18.6	1489	2.0
1173	17.4	768	
1263	15.8	395	
1434	13.3	86	
1549	11.9	39	
1151	8.0	2328	
1259	6.9	806	
1372	6.1	311	
1458	5.6	150	
1547	4.9	73	
1289	1.6	2199	
1374	1.5	854	
1398	1.4	676	
1434	1.3	469	
1511	1.2	241	
1594	1.1	119	
1667	1.0	74	
1051	33.9	1485	1.0
1107	30.6	930	
1206	29.3	373	
1362	25.4	93	
1131	8.4	2378	
1230	8.5	895	
1290	7.4	481	
1389	6.7	162	
1518	5.8	58	
1328	0.9	1268	
1373	0.9	637	
1426	0.8	287	
1469	0.7	157	
1533	0.7	84	
1121	19.3	1755	0.5
1194	18.4	800	
1278	18.0	314	
1351	16.9	129	
1444	15.6	53	
1157	8.6	1976	
1227	8.3	896	
1324	8.0	253	
1384	7.6	106	
1434	7.0	62	
1297	1.0	1196	
1325	1.0	732	
1342	1.0	671	
1360	0.9	501	
1426	0.9	237	
1441	0.8	146	
1504	0.8	67	
1106	32.4	1739	0.3
1185	31.1	780	
1278	29.7	213	
1331	28.7	95	
1413	26.2	46	
1163	8.6	1978	
1242	8.2	752	
1301	7.8	319	
1379	7.5	85	
1427	6.9	55	
1252	1.1	2022	
1287	1.0	996	
1323	1.0	529	
1357	1.0	386	
1370	1.0	293	
1431	0.9	144	
1500	0.9	84	
	Natural gas blend 3		
1019	20.2	1915	2.0
1045	19.6	1500	
1101	18.2	878	

Table 3 (*Continued.*)

T (K)	p (atm)	τ_{ign} (μs)	ϕ
1209	17.0	344	
1317	15.2	146	
1401	14.5	69	
1477	12.6	37	
1104	8.2	2126	
1139	8.1	1381	
1189	7.8	864	
1282	7.6	361	
1334	6.7	245	
1440	6.4	94	
1508	5.3	54	
1285	1.6	1055	
1320	1.6	948	
1388	1.4	446	
1482	1.4	221	
1555	1.2	107	
1604	1.1	78	
995	34.8	1944	1.0
1047	33.2	1074	
1114	31.9	541	
1212	30.2	205	
1319	26.9	84	
1170	8.5	1037	
1249	7.6	445	
1361	6.7	126	
1470	6.3	58	
1299	0.9	1008	
1311	0.9	766	
1265	0.8	1478	
1358	0.8	507	
1378	0.9	348	
1421	0.8	214	
1446	0.8	158	
1475	0.8	101	
1530	0.7	63	
1064	20.8	2168	0.5
1126	19.7	1107	
1192	18.5	535	
1310	16.8	139	
1369	15.6	65	
1467	14.6	20	
1146	8.7	1454	
1263	8.3	306	
1349	7.7	102	
1428	6.9	29	
1228	1.0	1695	
1268	1.0	899	
1298	1.0	498	
1306	0.9	517	
1356	0.9	266	
1411	0.9	135	
1084	33.7	1494	0.3
1131	33.0	913	
1178	30.7	557	
1279	29.8	138	
1354	27.0	58	
1152	8.7	1428	
1236	8.4	497	
1257	6.2	397	
1315	8.1	120	
1403	7.4	45	
1472	6.9	21	
1212	0.9	1410	
1219	1.0	1570	
1250	1.0	882	
1274	0.9	685	
1282	1.0	464	
1293	1.0	372	
1296	0.8	418	
1346	1.0	172	
1353	0.9	173	

Table 3 (*Continued.*)

T (K)	p (atm)	τ_{ign} (μs)	ϕ
1366	0.9	110	
1370	0.8	105	
1381	0.9	103	
1444	0.9	47	

5–8. Again, the agreement between model and experiment is very good over the whole range of temperature, pressure, and stoichiometry. The agreement is noticeably best for the stoichiometric and rich mixtures (Figs. 7 and 8), but some improvements can be made for the leaner mixtures (Figs. 5 and 6) at pressures around 1 and 8 atm. With such a wide range of available data, cross comparisons can be made between data groupings to gauge the effect of stoichiometry and mixture composition. Such comparisons are made in Sec. 3.3.

3.3 Discussion. General trends regarding the effect of fuel-to-air equivalence ratio on the ignition delay time can be seen by plotting several results for different ϕ but for the same fuel mixture and average pressure. Figure 9(*a*) presents both RCM and shock-tube ignition-time results for NG2 at an average pressure near 10 atm. A higher pressure is represented in Fig. 9(*b*), which displays data for NG2 at an average pressure around 20 atm. Note that the data in Figs. 9(*a*) and 9(*b*) represent equivalence ratios ranging from 0.5 up to 2.0. With this range in mind, one result that can be taken from the comparisons is that the variation in ϕ does not seem to have as much of an effect on τ_{ign} as changes in pressure do (as seen in Figs. 1–8). This minimal lack of sensitivity to ϕ holds over the entire range of temperatures, from about 700 K to 1600 K for both pressures in Fig. 9. For example, a factor of

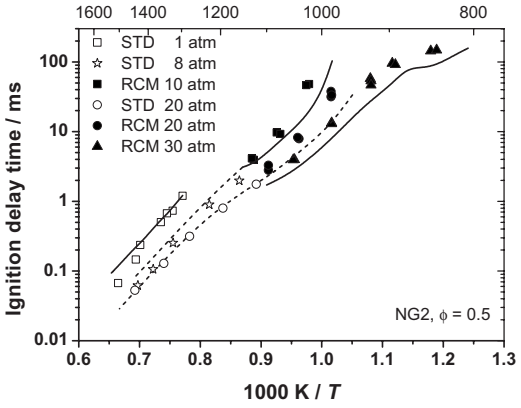

Fig. 1 Effect of pressure for NG2 mixture, ϕ=0.5 in air. Points are experimental results, and lines are model simulations. Dashed lines correspond to data at 8 atm and 20 atm.

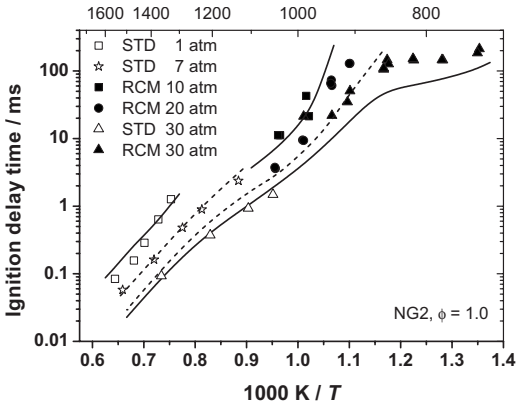

Fig. 2 Effect of pressure for NG2 mixture, ϕ=1.0 in air. Points are experimental results, and lines are model simulations. Dashed lines correspond to *P*=7 and 20 atm.

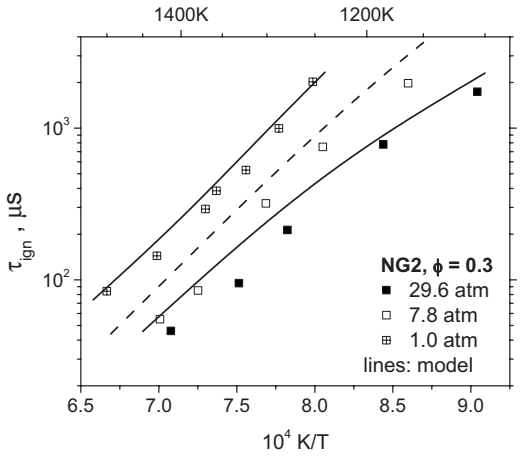

Fig. 3 Shock-tube ignition data and comparison to model for NG2, ϕ=0.3

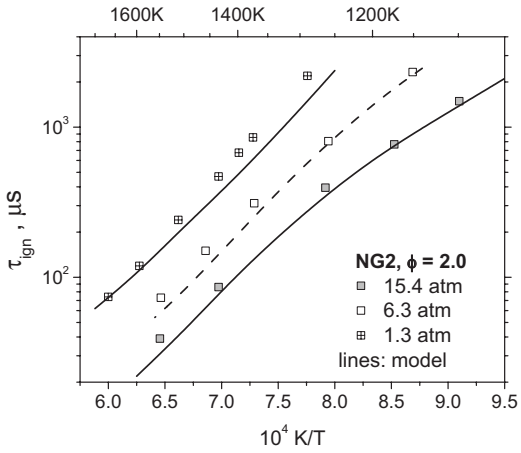

Fig. 4 Shock-tube ignition data and comparison to model for NG2, ϕ=2.0

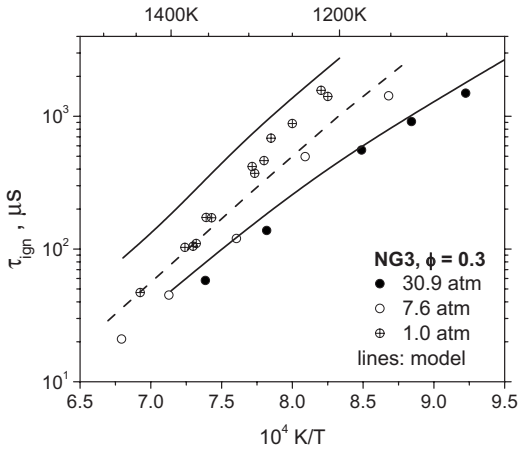

Fig. 5 Fuel-lean ignition delay time data from the shock-tube experiments and comparison to model for NG3, ϕ=0.3; dashed line: 7.6 atm

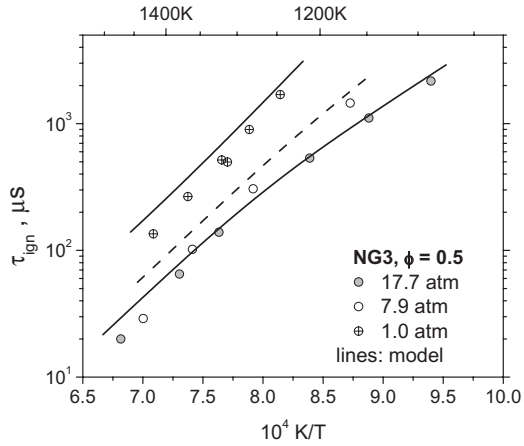

Fig. 6 Lean ignition delay time data from the shock-tube experiments and comparison to model for NG3, ϕ=0.5

4 change in ϕ from 0.5 to 2.0 at about 1400 K in Fig. 9(*b*) results in a change in ignition time of less than 50%. Conversely, at 1400 K for the same NG2 blend in Fig. 4, a factor of 4 change in pressure results in a change in τ_{ign} of about 200%.

Figures 9(*a*) and 9(*b*) also highlight the importance of the point of transition from low-to high-temperature kinetics; at low temperatures, fuel-rich mixtures are faster to ignite relative to fuel-lean mixtures, while lean mixtures ignite faster than rich mixtures at higher temperatures. At 10 atm, Fig. 9(*a*), the experimental data show that this point of transition occurs around 1212 K, while at 20 atm, Fig. 9(*b*), this transition also occurs but shifts to the higher temperature of 1250 K. This transition from low-to high-temperature kinetics is accurately reproduced by the kinetic mechanism in both figures. Moreover, because these experiments are measured close to and at the point of transition, there is observed a very small dependence on equivalence ratio for all three mixtures.

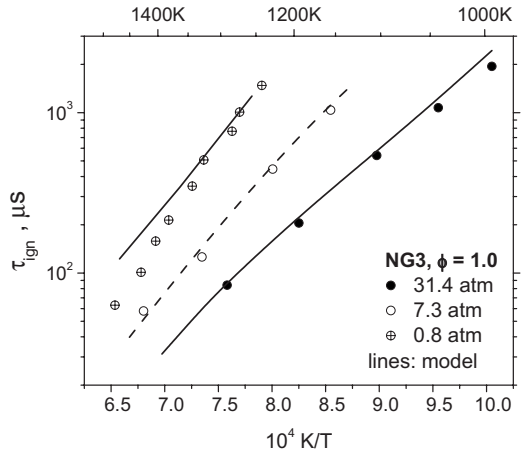

Fig. 7 Stoichiometric ignition delay time data from the shock-tube experiments and comparison to model for NG3, ϕ=1.0

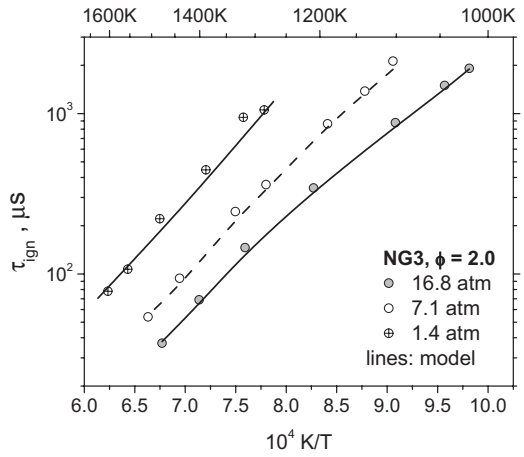

Fig. 8 Fuel-rich ignition delay time data from the shock-tube experiments and comparison to model for NG3, ϕ=2.0

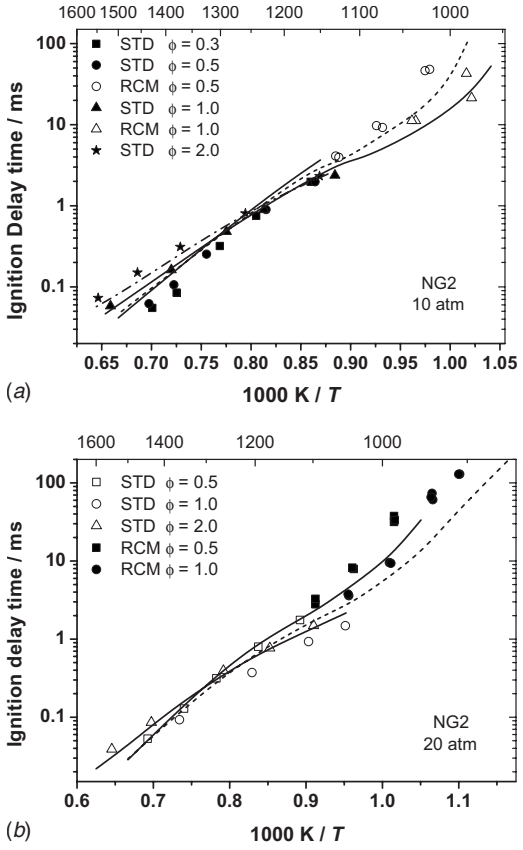

Fig. 9 Effect of equivalence ratio for the NG2 mixture using both shock-tube and RCM data. Points are experimental results, and lines are model simulations. Dashed lines correspond to ϕ=1.0.(*a*) Pressure≈10 atm. (*b*) Pressure≈20 atm.

Also with regard to the lower-temperature behavior, Figs. 1 and 2 show the effect that higher-order hydrocarbons have on ignition delay times; particularly in the RCM data at 30 atm, a region of reduced reactivity is observed in the temperature range 850–900 K at ϕ=0.5 (Fig. 1) and in the temperature range 720–850 K at ϕ=1.0 (Fig. 2). This "negative dependence" or at least zero dependence on temperature is due to the characteristic low- and intermediate-temperature chemistry associated with the larger hydrocarbons (C_3H_8, C_4H_{10}, and C_5H_{12}) present in the mixture, in which alkyl radicals from the fuel add to molecular oxygen and undergo intramolecular isomerization reactions, which lead to chain branching and/or propagation processes and which is responsible for the characteristic and complex negative temperature coefficient behavior associated with alkane fuels.

As seen in earlier studies on methane-based ignition [5–13], the addition of heavier hydrocarbons tends to have an accelerating effect on ignition. The results of the present study also show this trend. Figure 10 displays shock-tube ignition delay times comparing NG2 to NG3 at average pressures of 1 atm (Fig. 10(*a*)) and 30 atm (Fig. 10(*b*)). Also shown in Figs. 10(*a*) and 10(*b*) are calcu-

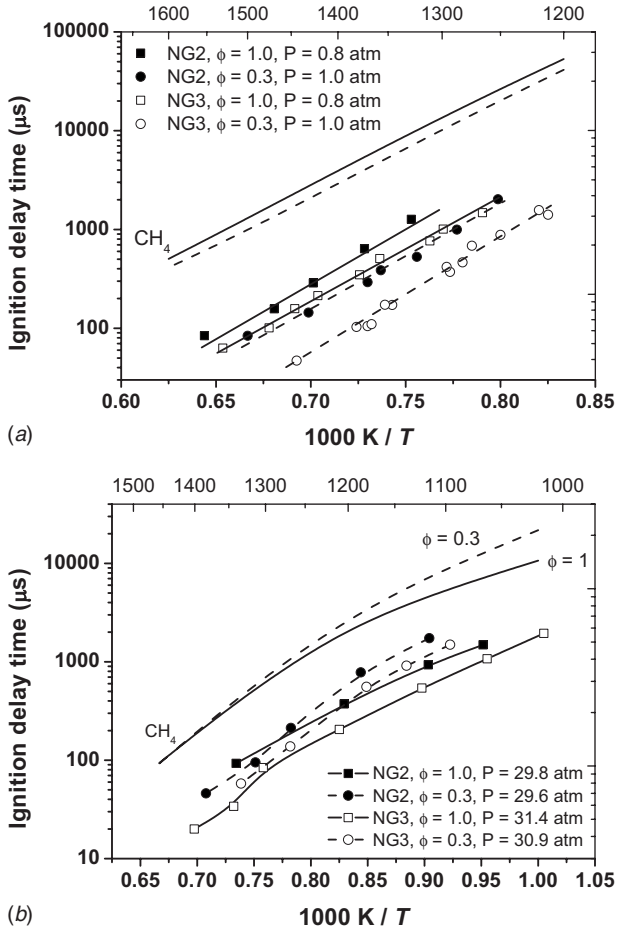

Fig. 10 Effect of mixture composition using shock-tube ignition delay time data. Points are experimental results; lines through data points are best fit lines, for clarity in deducing the trends; lines representing pure methane are model calculations. Solid lines correspond to ϕ=1.0, and dashed lines correspond to ϕ=0.3. (*a*) Pressure≈1 atm. (*b*) Pressure ≈30 atm.

lated ignition delay times for a pure methane fuel to highlight the relative effect of the heavier hydrocarbons. Each plot also shows two different equivalence ratios (0.3 and 1.0). The results in Fig. 10 indicate that, as expected, the NG3 blend, containing a greater amount of higher hydrocarbons than NG2, leads to faster ignition. This conclusion appears to hold over the entire range of ϕ, T, and P represented in Fig. 10. When compared with pure methane, the ignition of the NG2 and NG3 fuel blends are faster by a factor of 5 or more. Note, however, the somewhat diminished effect between NG2 and NG3 as compared with the much larger difference in ignition between the pure methane fuel and NG2.

One general trend evident in the data is that at higher temperatures and lower pressures, lean mixtures tend to ignite faster than rich mixtures, while at lower temperatures and higher pressures, the opposite is true. This trend is evident in the plots in Fig. 9 that show comparisons of equivalence ratio over a wide range of temperature. Figure 10 provides other stark examples; in Fig. 10(*a*), the conditions are near 1 atm, and the lean mixtures ignite faster (ϕ=0.3 compared with ϕ=1.0). In Fig. 10(*b*) at a higher pressure near 30 atm, it is the ϕ=1.0 mixtures that have the faster ignition when compared with ϕ=0.3. Increased fuel at lower temperatures and higher pressures actually contributes more to the chain branching than an increase in fuel concentration at higher temperatures.

At the lower temperatures (and higher pressures) throughout the negative coefficient regime, the alkyl radicals formed from the fuel add to molecular oxygen generating alkylperoxyl radicals (RO_2). These radicals then undergo an intramolecular isomerization reaction to generate a hydroperoxyl-alkyl radical (QOOH). At low temperatures, this radical adds to molecular oxygen generating a peroxyl-alkylhydroperoxide radical (O_2QOOH), which undergoes an intramolecular isomerization reaction and ultimately yields two reactive hydroxyl radicals and an alkoxyhydroperoxide radical. Thus, at low temperatures this process generates three reactive radicals from one fuel alkyl radical, with the fuel alkyl radical concentration being the rate determining parameter.

As the temperature increases, propagation reactions of the hydroperoxyl-alkyl radicals (QOOH) become competitive with the addition to molecular oxygen (which leads to chain branching), and thus fuel reactivity decreases leading to negative temperature coefficient behavior.

4 Laminar Flame Speeds

As mentioned above, laminar flame speed is a key parameter for gauging the effect of fuel variations on the coupling between the chemistry and diffusion. Laminar flame speed can also be tied to the Markstein length and flame dynamics via the flame stretch and strain. Presented in this section are details on the experiment used to obtain the flame speed for the NG2 and NG3 mixtures (Table 1), followed by the measured results and their comparison to the detailed kinetics model.

4.1 Experiment. All experiments were conducted in an AL7075 cylindrical bomb with an inner diameter of 30 cm and internal length of 36.2 cm. The walls are 3.18-cm thick. Both ends contain a fused quartz window of 20.3 cm diameter and 6.3-cm thick. More detail on the experimental setup is given in Ref. [37]. Both pressure and temperature are constantly monitored during the experiment, and the pressure signals are stored in a 14-bit, 5-MHz data acquisition board. The experiments are conducted behind a protective blast wall, and four pneumatic ball valves allow for remote operation of the apparatus. The vessel is rated up to 300 bars, and rupture disks are installed for overpressure protection.

A Z-type Schlieren setup, as described by Settles [38], is used for monitoring the freely propagating flames. Two $f/8$ 15.2-cm diameter mirrors in combination with a mercury light source are used for the Schlieren setup. A circular knife edge in the form an adjustable aperture is used instead of the conventional vertical "flat" knife edge techniques. It can be shown that this gives a more uniform flame front for axisymmetric phenomena [37]. The flame propagation is captured using a high-speed digital camera (Cooke Corp. PCO 1200 hs) with a frame rate of around 2000 fps.

Ignition of the mixture is accomplished by using a combination of an automotive ignition coil, a capacitor, and a constant-current power supply. In this way, the ignition energy can be minimized for each individual mixture. Two copper electrodes leave a spark gap of less the 1 mm.

Experiments were conducted at initial pressures up to 4 atm for methane, NG2, and NG3 over equivalence ratios of 0.7–1.3. The mixtures were created using partial pressures in a separate mixing tank similar to that described by Ref. [31]. This homogeneous mixture in the tank could be used for conducting several experiments depending on the initial pressure required. Prior to each run, the flame speed vessel was evacuated to less than 50 mTorr before being filled with the required mixture. The mixture was then allowed to cool down from the compression heating until the temperature in the vessel was within 0.5°C of the room temperature, which was typically at 25°C. The methane experiments were repeated at least five times and averaged per data point, and the NG2 and NG3 mixtures were repeated three to four times and then averaged.

Each experiment was initiated by sending a signal to the ignition system, the digital oscilloscope, and the digital camera. The

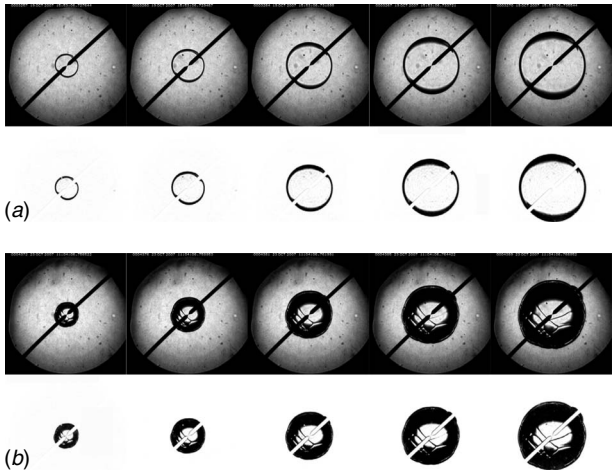

Fig. 11 Schlieren photographs of NG2/air with and without background subtraction, ϕ=1.0; frame width is 12 cm. (*a*) Pressure=1 atm. (*b*) Pressure=4 atm.

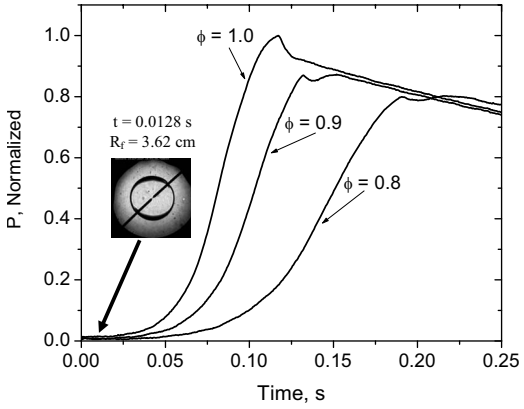

Fig. 12 Pressure histories of CH_4/air mixtures for equivalence ratios of 0.8, 0.9, and 1.0; P_i=1 atm, T_i=298 K. All images used in the data reduction are taken before significant pressure rise.

camera is then manually stopped, and the images containing the flame propagation are saved. Flame radius versus time is obtained from the stored images by using special image-tracking software [39]. Radii less than 0.5 cm were discarded to avoid any potential spark disturbances.

Note that the optical components described herein allow for a large aperture (>10 cm). For low-pressure experiments, the full 0.5–5 cm radius range can be utilized. For higher-pressure experiments where wrinkles were observed, a radius of up to 2.5 cm was used. This limiting radius compares well against other studies conducted at similar pressures.

Figures 11(*a*) and 11(*b*) show the flame propagation of NG2 for 1 atm and 4 atm, respectively. For both cases, the images are shown as recorded and then the initial flameless image is subtracted, leaving just the flame. It can be seen in Fig. 11(*b*) that there are spark- or electrode-induced wrinkles on the surface of the flame. It was shown by Rozenchan et al. [40] that self-similar propagation of such wrinkles suggests that the linear relation between flame speed and flame stretch still holds. Since it can be seen that a new wrinkle is being formed between R=3.0 and 3.5 cm, the radius was only used up to 2.5 cm for this study for elevated pressures, as mentioned above. Cell cracking was not observed in this study. The O_2/N_2 ratio was always 21/79, and the dilution level (i.e., the Lewis number) was never changed herein, but will possibly be necessary in the future for experiments conducted at initial pressures higher than 4 atm.

It is important to show that the pressure rise during the experiments is negligible during the collection of the flame images. The decrease in flame speed at higher pressures would indicate an artificial decrease in Markstein length (flame speed versus flame stretch dependency) over the period that flame speed is recorded during a pressure increase. Figure 12 shows the pressure traces recorded for CH_4/air for three different equivalence ratios (0.8, 0.9, and 1.0). The position of the flame relative to the pressure is also shown. It can be seen that the pressure rise is negligible during the collection of the data.

The proposed linear relationship between flame speed and flame stretch [41–43] was used herein to obtain the unstretched flame speed

$$S_b = S_b^0 - L_b\alpha \tag{1}$$

where S_b is the stretched flame speed, S_b^0 is the unstretched flame speed, L_b is the burned Markstein length, and α is the flame stretch defined by

$$\alpha = \frac{1}{A}\frac{dA}{dt} = \frac{1}{4\pi R^2}\frac{d(4\pi R^2)}{dt} = \frac{2}{R}\frac{dR}{dt} \tag{2}$$

Equation (1) can be integrated to obtain Eq. (3)

$$R = S_b^0 t - 2L_b \ln(R) + \text{const} \tag{3}$$

This equation can then be used to obtain the unstretched flame speed and the Markstein length through linear regression. This approach is preferred over using finite difference to obtain the instantaneous flame speed, since small perturbations in flame radius can cause major changes in slope. Using the linear regression method averages out this problem.

4.2 Flame Speed Results. As mentioned above, three different mixtures, CH_4, NG2, and NG3, were used over equivalence ratios from 0.7 to 1.3 at 1 atm. Pressure dependency of the NG2 mixture was also obtained for pressures of up to 4 atm. All data are compared against the kinetics model described above and are used to compare with the ignition delay time data. All initial temperatures were 298 ± 1 K. The experimental results can be found in Table 4.

As validation of the experimental technique and the laminar flame speed results, the CH_4 results can be compared with the established literature since the laminar flame speeds for methane at 1 atm are very well known. A convenient way of doing this is to compare the measured data for pure methane with the prediction of the GRI 3.0 chemical kinetics mechanism [27]. This particular mechanism was validated using the methane flame speed database and has been shown to replicate the measured results very well. The present data for methane at 1 atm are shown in comparison to the accurate predictions of GRI 3.0 in Figs. 13(*a*) and 13(*b*). As seen in these figures of S_L versus the equivalence ratio, the agreement between the present data and GRI 3.0 is excellent.

Figure 13(*a*) shows the burning velocity of CH_4 and NG2 for equivalence ratios of 0.7–1.3 at 1 atm. It can be seen that the NG2 mixture shows a slight acceleration over the whole range of equivalence ratios with a minimum effect at stoichiometric conditions. From the model, the difference in predicted burning velocity between CH_4 and NG2 is minimal in the fuel-lean region, and the two predictions diverge when the mixtures become more fuel rich. The model slightly overpredicts the flame speed for lean methane flames and agrees well with lean NG2 flames. For rich flames, the model underpredicts the experimental results for both the pure methane as the NG2 flames, where the effect is less profound for the later.

Figure 13(*b*) shows the burning velocity of CH_4 and NG3 mixtures at 1 atm. The experimental results indicate that the effect of the higher level of higher-order hydrocarbons (38.75% of the total fuel) has a marginal effect in the fuel-lean regime as compared

Table 4 Experimental results for laminar flame speed, S_L, for CH_4, NG2, and NG3; T_i=298 K

CH_4/air, P=1 atm	
ϕ	S_L (cm/s)
0.7	15.0
0.8	23.7
0.9	30.0
1	35.1
1.1	34.7
1.2	31.3
1.3	24.7

NG2/air, P=1 atm	
ϕ	S_L (cm/s)
0.7	17.1
0.9	31.2
1.1	37.2
1.2	35.6
1.3	28.0

NG3/air, P=1 atm	
ϕ	S_L (cm/s)
0.7	19.2
0.8	25.8
0.9	31.4
1	36.0
1.1	38.0
1.2	36.1
1.3	30.2

NG3/air, ϕ=1.0	
P (atm)	S_L (cm/s)
1.0	36.1
1.5	32.0
1.8	31.0
2.0	30.1
2.4	28.4
2.5	28.2
4.0	24.4

with the NG2 experimental results. However, for fuel-rich mixtures, the burning velocity is higher than that recorded for the pure CH_4 flames as well as for the NG2 flames. The model shows similar behavior as for the NG2 mixture, where the agreement under lean conditions is acceptable, and where the model deviated for the experimental results for rich conditions for both the pure CH_4, as well as the NG3 mixture.

The burning velocity of NG2 is plotted against pressure in Fig. 14 for pressures between 1 atm and 4 atm. The predicted burning velocity for stoichiometric CH_4 by GRI 3.0 [27] is also plotted, as well as the model prediction of the NG2 and NG3 mixtures using the present kinetics model. It can be seen that the experimental results show a burning velocity that is slightly higher than the prediction of CH_4 by GRI 3.0. The current model underpredicts the flame speed for the NG mixture and shows burning velocities that are slightly less than the predicted CH_4 burning velocities. The model prediction of the NG3 mixture is slightly faster than the NG2 mixture.

5 Discussion

Given the increasing importance of fuel flexibility for power generation applications, the present study is especially important for the gas turbine and combustion communities for several reasons: (1) a comprehensive database of ignition delay times that cover a wide range of stoichiometry, temperature, and pressure

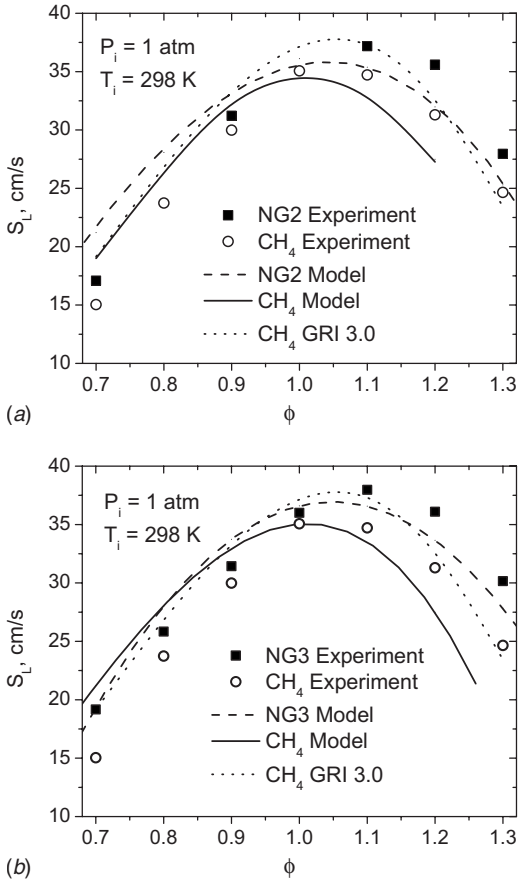

Fig. 13 Measured laminar burning velocities and comparison to model predictions for P_i=1 atm, T_i=298 K. (*a*) Methane and NG2 in air. (*b*) Methane and NG3 in air.

was produced; (2) a detailed chemical kinetics model that does a remarkable job over such a comprehensive range of conditions was presented; (3) high-pressure laminar flame speed results are also available for a similar range of fuel blend composition and stoichiometry; (4) a range of methane-hydrocarbon blends including methane concentrations as low as 62.5% by volume was explored; and (5) two experimental ignition techniques—shock tube and rapid compression machine—were combined to provide a full range of temperatures from about 700 K to 1600 K at engine pressures.

As seen in the ignition delay time results in Figs. 1–8, the strong ability of the kinetics model to reproduce the correct trends

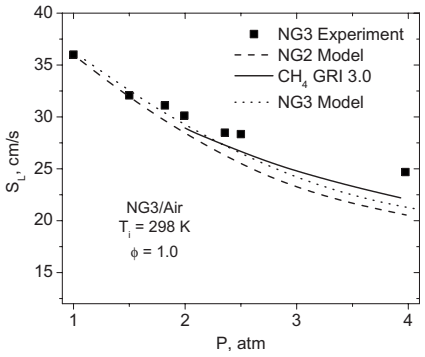

Fig. 14 Pressure dependence of the laminar burning velocity for NG2 experiments and comparison to model for CH_4, NG2, and NG3. ϕ=1.0, T_i=298 K.

both qualitatively and in absolute magnitude cannot be overstated, particularly when one considers the range of mixtures and conditions considered. The model seems to be best at stoichiometric and rich conditions, even for pressures as high as 30 atm. Nonetheless, the same figures point out some areas for improvement. For example, at the lowest temperatures, the model tends to underpredict the ignition times by as much as a factor of 2 or more. Other improvements can be made at the leanest conditions examined at the lower pressures, Figs. 5–7. One area of kinetic interest not covered by the present study is the effect of ethane and other hydrocarbons for extreme levels of them in the fuel blend, i.e., for methane contents between 60% and 0% by volume. Additional work in the area of methane-hydrocarbon kinetics would also include sensitivity analyses over the range of conditions herein, including the regions of lesser agreement between model and data, to determine the dominant reactions and pathways.

For the laminar flame speed results, the quantitative agreement between model and experiment is not as good as for the ignition times, although the basic trends with composition, pressure, and ϕ are captured. The disagreement is seen in Figs. 13 and 14, particularly at the richer conditions and at pressures greater than 1 atm. This disagreement is not too surprising, however, since the present model was tuned mostly using the ignition delay time experiments and not with the current S_L results. Note that the GRI-MECH 3.0 predictions for the pure methane case are actually better on the rich side than the present model. Since flame speeds depend not only on the chemical kinetics but also on the diffusive properties of the reactive mixtures; a careful assessment of the transport data utilized in the present model should be made in light of the results herein.

A comprehensive sensitivity analysis to identify what needs to be changed in the present mechanism to obtain better agreement between model and data is currently underway in the authors' laboratories. The results of this analysis along with the improved kinetics mechanism will be presented in a future paper.

Finally, future S_L experiments should include a wider range of pressure. However, care should be taken when moving to higher pressures since at pressures above about 4 atm in the present experiments, instabilities start to form, leading to wrinkling of the flame and inevitably faster flame speeds due to the corresponding increase in turbulence. Wrinkling of the flame front at elevated pressures can be mitigated by altering the Lewis number of the mixture (by adding different dilution gases to the fuel-air mixture). Higher-temperature experiments are also needed but will require heating of the facility to higher initial temperatures, T_i. Due to its relation to flame dynamics, additional work should concentrate on the Markstein length and its sensitivity to fuel composition.

6 Summary

Experiments and kinetics modeling were performed for two methane-based fuel blends containing relatively large levels of higher-order hydrocarbons (ethane, propane, n-butane, and pentane). The experiments included ignition delay times from shock tubes and a rapid compression machine, as well as laminar flame speed measurements from a high-pressure vessel with optical access. Conditions representative of gas turbine engines were emphasized, including pressures from 0.7 atm to 33.9 atm for undiluted fuel-air mixtures over a wide range of equivalence ratios (0.3–2.0). The combination of shock tube and rapid compression machine allowed ignition delay times to be obtained over a range of temperatures from 739 K to 1667 K.

The ignition delay time results compare favorably with the detailed kinetics model over a wide range of conditions, including pressures on the order of 30 atm and for the fuel-rich conditions. Additionally, the shock-tube and rapid compression machine results are complementary. As expected, the fuel blend with the larger percentage of higher-order hydrocarbons produced the faster ignition, and the ignition seems to depend more on the pressure than on the fuel-air stoichiometry. Some areas for improvement to the kinetics model were identified.

Laminar flame speeds for both natural gas blends, as well as a baseline pure methane fuel, were obtained at 1 atm initial pressure over a range of equivalence ratios from 0.7 to 1.31. In general, the flame speeds for the fuel blends were smaller than for the pure methane results, ranging from about 10% at lean conditions to as much as 40–50% for rich mixtures. At 1 atm, the kinetics model tends to agree well with the measured flame speeds on the lean side but underpredicts the flame speed for rich mixtures. A pressure excursion up to 4 atm was done for a stoichiometric fuel-air mixture, with S_L decreasing with increasing pressure. The model tended to under predict S_L by as much as 25% at 4 atm. Suggestions for future flame speed research for methane-hydrocarbon blends were also presented.

Acknowledgment

The work herein was sponsored primarily by Rolls-Royce Canada and in part by the National Science Foundation under Contract No. CBET-0832561. Additional support provided by The Aerospace Corporation. The assistance of Benjamin Corbin, Alexander Barrett, and Matthew Davis (UCF) in the laboratory is appreciated.

References

[1] Bourque, G., Healy, D., Curran, H., Simmie, J., de Vries, J., Antonovski, V., Corbin, B., Zinner, C., and Petersen, E., 2007, "Effect of Higher-Order Hydrocarbons on Methane-Based Fuel Chemistry at Gas Turbine Pressures," ASME Paper No. GT2007-28039.
[2] Lieuwen, T., McDonell, V., Petersen, E., and Santavicca, D., 2008, "Fuel Flexibility Influences on Premixed Combustor Blowout, Flashback, Autoignition, and Stability," ASME J. Eng. Gas Turbines Power, **130**, p. 011506.
[3] Lieuwen, T., 2003, "Modeling Premixed Combustion-Acoustic Wave Interactions: A Review," J. Propul. Power, **19**, pp. 837–846.
[4] Bradley, D., Hicks, R. A., Lawes, M., Sheppard, C. G. W., and Woolley, R., 1998, "The Measurement of Laminar Burning Velocities and Markstein Numbers for Iso-Octane–Air and Iso-Octane–n-Heptane–Air at Elevated Temperatures and Pressures in an Explosion Bomb," Combust. Flame, **115**, pp. 126–144.
[5] Higgin, R. M. R., and Williams, A., 1969, "A Shock-Tube Investigation of the Ignition of Lean Methane and n-Butane Mixtures With Oxygen," Proc. Combust. Inst., **12**, pp. 579–590.
[6] Crossley, R. W., Dorko, E. A., Scheller, K., and Burcat, A., 1972, "The Effect of Higher Alkanes on the Ignition of Methane-Oxygen-Argon Mixtures in Shock Waves," Combust. Flame, **19**, pp. 373–378.
[7] Eubank, C. S., Rabinowitz, M. J., Gardiner, W. C., Jr., and Zellner, R. E., 1981, "Shock-Initiated Ignition of Natural Gas-Air Mixtures," Proc. Combust. Inst., **18**, pp. 1767–1774.
[8] Zellner, R., Niemitz, K. J., Warnatz, J., Gardiner, W. C., Jr., Eubank, C. S., and Simmie, J. M., 1983, "Hydrocarbon Induced Acceleration of Methane-Air Ignition," Prog. Astronaut. Aeronaut., **80**, pp. 252–272.
[9] Spadaccini, L. J., and Colket, M. B., III, 1994, "Ignition Delay Characteristics of Methane Fuels," Prog. Energy Combust. Sci., **20**, pp. 431–460.
[10] Naber, J. D., Siebers, D. L., Di Julio, S. S., and Westbrook, C. K., 1994, "Effects of Natural Gas Composition on Ignition Delay Under Diesel Conditions," Combust. Flame, **99**, pp. 192–200.
[11] Griffiths, J. F., Coppersthwaite, D., Phillips, C. H., Westbrook, C. K., and Pitz, W. J., 1990, "Auto-Ignition Temperatures of Binary Mixtures of Alkanes in a Closed Vessel: Comparisons Between Experimental Measurements and Numerical Predictions," Proc. Combust. Inst., **23**, pp. 1745–1752.
[12] Huang, J., and Bushe, W. K., 2006, "Experimental and Kinetic Study of Autoignition in Methane/Ethane/Air and Methane/Propane/Air Mixtures Under Engine-Relevant Conditions," Combust. Flame, **144**, pp. 74–88.
[13] Petersen, E. L., Hall, J. M., Smith, S. D., de Vries, J., Amadio, A. R., and Crofton, M. W., 2007, "Ignition of Lean Methane-Based Fuel Blends at Gas Turbine Pressures," ASME J. Eng. Gas Turbines Power, **129**, pp. 937–944.
[14] Petersen, E. L., Kalitan, D. M., Simmons, S., Bourque, G., Curran, H. J., and Simmie, J. M., 2007, "Methane/Propane Oxidation at High Pressures: Experimental and Detailed Chemical Kinetic Modeling," Proc. Combust. Inst., **31**, pp. 447–454.
[15] Petersen, E. L., and de Vries, J., 2005, "Measuring the Ignition of Fuel Blends Using a Design of Experiments Approach," AIAA Paper No. 2005-1165.
[16] de Vries, J., and Petersen, E. L., 2005, "Design and Validation of a Reduced Test Matrix for the Autoignition of Gas Turbine Fuel Blends," ASME Paper No. IMECE2005-80040.
[17] de Vries, J., and Petersen, E. L., 2007, "Autoignition of Methane-Based Fuel Blends Under Gas Turbine Conditions," Proc. Combust. Inst., **31**, pp. 3163–3171.

[18] Healy, D., Dooley, S., Curran, H. J., Petersen, E., Simmons, S., Kalitan, D., Bourque, G., and Simmie, J. M., 2006, "A Rapid Compression Machine Study of Natural Gas Mixtures," Work in Progress Poster 4E-05: 31st International Symposium on Combustion, Heidelberg, Germany, Aug. 6–11.
[19] Eschenbach, R. C., and Agnew, J. T., 1958, "Use of a Constant-Volume Bomb Technique for Measuring Burning Velocity," Combust. Flame, **2**, pp. 273–285.
[20] Agrawal, D. D., 1981, "Experimental Determination of Burning Velocity of Methane-Air Mixtures in a Constant Volume Vessel," Combust. Flame, **42**, pp. 243–252.
[21] Egolfopoulos, F. N., Cho, P., and Law, C. K., 1989, "Laminar Flame Speeds of Methane-Air Mixtures Under Reduced and Elevated Pressures," Combust. Flame, **76**, pp. 375–391.
[22] Savarianandam, V. R., and Lawn, C. J., 2006, "Burning Velocity of Premixed Turbulent Flames in the Weakly Wrinkled Regime," Combust. Flame, **146**, pp. 1–18.
[23] Hessler, J. P., 1998, "Calculation of Reactive Cross Sections and Microcanonical Rates From Kinetic and Thermochemical Data," J. Phys. Chem. A, **102**, pp. 4517–4526.
[24] You, X., Wang, H., Goos, E., Sung, C.-J., and Klippenstein, S. J., 2007, "Reaction Kinetics of $CO+HO_2 \rightarrow$ Products: Ab Initio Transition State Theory Study With Master Equation Modeling," J. Phys. Chem. A, **111**, pp. 4031–4042.
[25] Srinivasan, N. K., Michael, J. V., Harding, L. B., and Klippenstein, S. J., 2007, "Experimental and Theoretical Rate Constants for $CH_4+O_2 \rightarrow CH_3+HO_2$," Combust. Flame, **149**, pp. 104–111.
[26] Jasper, A. W., Klippenstein, S. J., and Harding, L. B., 2007, "Theoretical Rate Coefficients for the Reaction of Methyl Radical and Hydroperoxyl Radical and for Methyl-Hydroperoxide Decomposition," private communication.
[27] Smith, G. P., Golden, D. M., Frenklach, M., Moriarty, N. W., Eiteneer, B., Goldenberg, M., Bowman, C. T., Hanson, R. K., Song, S., Gardiner, W. C., Jr., Lissianski, V. V., and Qin, Z., http://www.me.berkeley.edu/gri_mech/.
[28] Curran, H. J., Gaffuri, P., Pitz, W. J., and Westbrook, C. K., 1998, "A Comprehensive Modeling Study of n-Heptane Combustion," Combust. Flame, **114**, pp. 149–177.
[29] Curran, H. J., Gaffuri, P., Pitz, W. J., and Westbrook, C. K., 2002, "A Comprehensive Modeling Study of Iso-Octane Oxidation," Combust. Flame, **129**, pp. 253–280.
[30] Kee, R. J., Rupley, F. M., Miller, J. A., Coltrin, M. E., Grcar, J. F., Meeks, E., Moffat, H. K., Lutz, A. E., Dixon-Lewis, G., Smooke, M. D., Warnatz, J., Evans, G. H., Larson, R. S., Mitchell, R. E., Petzold, L. R., Reynolds, W. C., Caracotsios, M., Stewart, W. E., Glarborg, P., Wang, C., and Adigun, O., 2001, "PREMIX: A Program for Modeling Steady, Laminar, One-Dimensional Premixed Flames," Reaction Design, Inc., San Diego, CA.
[31] Petersen, E. L., Rickard, M. J. A., Crofton, M. D., Abbey, E. D., Traum, M. J., and Kalitan, D. M., 2005, "A Facility for Gas- and Condensed-Phase Measurements Behind Shock Waves," Meas. Sci. Technol., **16**, pp. 1716–1729.
[32] Aul, C. J., de Vries, J., and Petersen, E. L., 2007, "New Shock-Tube Facility for Studies in Chemical Kinetics at Engine Conditions," Eastern States Fall Technical Meeting of the Combustion Institute, Charlottesville, VA, Oct. 21–24.
[33] Affleck, W. S., and Thomas, A., 1969, "An Opposed Piston Rapid Compression Machine for Preflame Reaction Studies," Proc. Inst. Mech. Eng., Part H: J. Eng. Med., **183**, pp. 365–385.
[34] Brett, L., MacNamara, J., Musch, P., and Simmie, J. M., 2001, "Simulation of Methane Autoignition in a Rapid Compression Machine With Creviced Pistons," Combust. Flame, **124**, pp. 326–329.
[35] Gallagher, S. M., Curran, H. J., Metcalfe, W. K., Healy, D., Simmie, J. M., and Bourque, G., 2008, "A Rapid Compression Machine Study of the Oxidation of Propane in the Negative Temperature Coefficient Regime," Combust. Flame, **153**, pp. 316–333.
[36] Lund, C. M., and Chase, L., 1995, "HCT-A General Computer Program for Calculating Time-Dependent Phenomena Involving One-Dimensional Hydrodynamics, Detailed Chemical Kinetics and Transport," Lawrence Livermore National Laboratory, Report No. UCRL-52504.
[37] De Vries, J., Corbin, B., and Petersen, E. L., "Construction of a High Pressure Flame Speed Facility," unpublished.
[38] Settles, G. S., 2006, *Schlieren and Shadowgraph Techniques*, 1st ed., Springer, Heidelberg, Germany.
[39] Klimek, R., and Wright, T., 2006, "Spotlight-8 Image Analysis Software," Report No. NASA/TM-2006-214084.
[40] Rozenchan, G., Zhu, D. L., Law, C. K., and Tse, S. D., 2002, "Outward Propagation, Burning Velocities, and Chemical Effects of Methane Flames Up to 60 atm," Proc. Combust. Inst., **29**, pp. 1461–1469.
[41] Markstein, G. H., 1964, *Non-Steady Flame Propagation*, Pergamon, New York.
[42] Dowdy, D. R., Smith, D. B., Taylor, S. C., and Williams, A., 1990, "The Use of Expanding Spherical Flames to Determine Burning Velocities and Stretch Effects in Hydrogen/Air Mixtures," Proc. Combust. Inst., **23**, pp. 325–332.
[43] Brown, J. M., McLean, I. C., Smith, D. B., and Taylor, S. C., 1996, "Markstein Lengths of CO/H2/Air Flames Using Expanding Spherical Flames," Proc. Combust. Inst., **26**, pp. 875–881.